JACS
JOURNAL OF THE AMERICAN CHEMICAL SOCIETY

Article

pubs.acs.org/JACS

Introducing Amphiphilicity to Noble Metal Nanoclusters via Phase-Transfer Driven Ion-Pairing Reaction

Qiaofeng Yao, Xun Yuan, Yong Yu, Yue Yu, Jianping Xie,* and Jim Yang Lee*

Department of Chemical and Biomolecular Engineering, National University of Singapore, 10 Kent Ridge Crescent, Singapore 119260

Supporting Information

ABSTRACT: Amphiphilicity is a surface property that has yet to be explored for the noble metal nanoclusters (NCs). This article shows how amphiphilicity may be added to sub-2-nm metal NCs by patching hydrophilic NCs (e.g., $Au_{25}(MHA)_{18}$ NCs where MHA is 6-mercaptohexanoic acid) with hydrophobic cations (e.g., cetyltrimethylammonium ion, CTA^+) to about half of a monolayer coverage. Specifically we demonstrate the preparation of amphiphilic $Au_{25}(MHA)_{18}$@xCTA NCs (x = 6–9 where x is the number of CTA^+ per NC) by the phase-transfer (PT) driven ion-paring reaction between CTA^+ and $-COO^-$ (derived from the deprotonation of the terminal carboxyl group of MHA). Due to the coexistence of flexible hydrophilic MHA and hydrophobic MHA···CTA ligands in comparable amounts on the NC surface, the $Au_{25}(MHA)_{18}$@xCTA NCs (x = 6–9) exhibit good amphiphilicity, which enabled them to dissolve in solvents with distinctly different polarities and to self-assemble like a molecular amphiphile. Consequently, the amphiphilic $Au_{25}(MHA)_{18}$@xCTA NCs (x = 6–9) could self-organize into stacked bilayers at the air–liquid interface, similar to the formation of lyotropic liquid crystalline phases by common surfactants. The good solubility and molecular-amphiphile-like self-assembly properties can significantly increase the utility of noble metal NCs in basic and applied research.

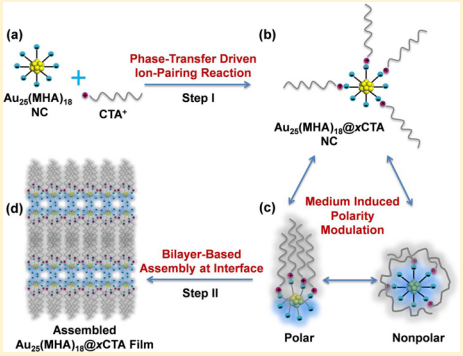

INTRODUCTION

Thiolate-protected noble metal nanoclusters (NCs), or $M_n(SR)_m$ (where M and SR are the metal atom and the thiolate ligands, respectively), are extremely small particles with a core size smaller than 2 nm.[1−4] They exhibit strong size-dependent properties such as a discrete electronic structure, intense photoluminescence, and high catalytic activity.[5−16] These properties can be additionally modified by surface engineering. For example, the electronic and optical properties of NCs can be varied by tailoring the ligand environment; and the critical role of the NC surface on molecular recognition has been well-documented.[11,17−26] Amphiphilicity is a NC surface property which has yet to be explored. Similar to amphiphilic nanoparticles,[27−29] an amphiphilic surface may impart NCs with good solubility in a wide range of solvents, thereby increasing their utility in basic and applied research. It also introduces molecular-amphiphile-like self-assembly properties (formation of spherical, cylindrical, or disk-shaped micelles,[27−30] vesicles,[31,32] and bilayers[33]) and packs the NCs into hierarchical structures with the desired geometry, symmetry, and long-range order for NC structural determination and further diversification of properties.[8,34−40] Amphiphilic NCs make it easier to study the difference between discrete and assembled NCs.

In principle, a good NC amphiphile (or amphiphilic NC) should possess a comparable number of hydrophilic and hydrophobic moieties on its surface.[30,41,42] Such amphiphilic NCs may be produced by two means: (1) ligand-exchange reaction[21,22,43−46] and (2) partial modification of a uniform surface. However, in the first approach where the creation of amphiphilicity relies on the exchange reaction between ligands with markedly different polarities, the metal core is often perturbed to result in random changes of the NC optical and catalytic properties.[44,46] A "soft" surface modification approach without perturbation of the metal core is clearly the alternative. This is best accomplished by partially patching the surface of hydrophilic NCs with hydrophobic moieties because hydrophilic ligands (e.g., carboxyl (−COOH) and sulfonic ($-SO_3H$)[24,47−49] are more amenable to surface modifications. Hydrophobic NCs, on the contrary, lack similar surface reactivity. Since most hydrophilic NCs deprotonate easily at or above pH 7 to acquire a negative charge, electrostatic interaction can be a means to drive the surface modification of hydrophilic NCs.[39,50,51]

Herein, we demonstrate the preparation of amphiphilic NCs by coating hydrophilic NCs with hydrophobic cations to about half of a monolayer coverage. This was made possible by a phase-transfer (PT) driven ion-paring reaction between hydrophobic cations (e.g., cetyltrimethylammonium, CTA^+) and the anionic surface groups of hydrophilic NCs (e.g., carboxylate, $-COO^-$). A moderately polar organic medium could then be used to selectively extract these moderately polar NCs (i.e., amphiphilic

Received: January 5, 2015
Published: January 13, 2015

DOI: 10.1021/jacs.5b00090
J. Am. Chem. Soc. 2015, 137, 2128−2136

Scheme 1. Schematic Illustration of the Synthesis of Amphiphilic $Au_{25}(MHA)_{18}$@*x*CTA NCs by the Phase-Transfer (PT) Driven Ion-Pairing Reaction

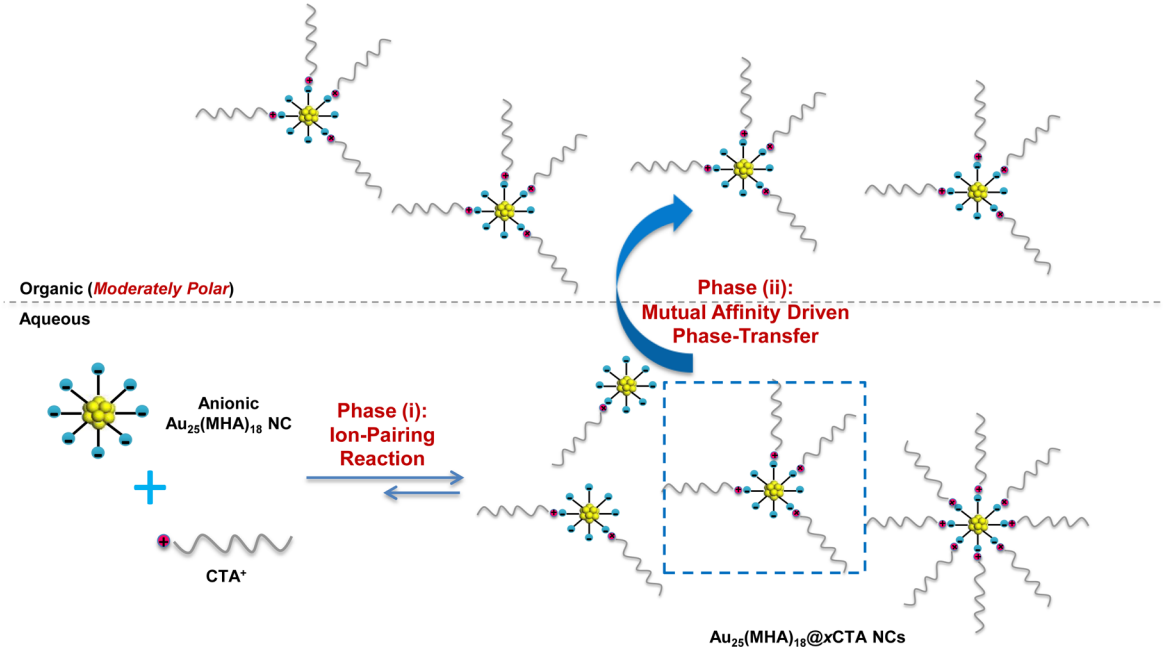

NCs) from the aqueous phase to a lyophilic phase, driving the ion-pairing reaction in the aqueous phase to continuously regenerate these amphiphilic NCs. The amphiphilic NCs formed as such were readily soluble in solvents spanning a wide range of relative dielectric constants (ε_r = 4.15−42.5). More interestingly, the amphiphilic NCs could be self-assembled into a stacked bilayer structure at the air−liquid interface, similar to the formation of lamellar liquid crystals from common amphiphilic molecules.[52,53]

RESULTS AND DISCUSSION

Synthesis of Amphiphilic $Au_{25}(MHA)_{18}$@*x*CTA NCs (*x* = 6−9). $Au_{25}(MHA)_{18}$ NCs (where MHA is 6-mercaptohexanoic acid) and CTA^+ were the model hydrophilic NCs and hydrophobic cations in this study, respectively. The binding of CTA^+ to the surface of the $Au_{25}(MHA)_{18}$ NCs was driven by the following ion-pairing reaction:[50,51]

$$CTA^+ + Na^+(^-OOC\text{-}) \rightleftarrows (CTA^+)(^-OOC\text{-}) + Na^+ \quad (1)$$

where $-COO^-$ was from the deprotonation of the −COOH group (one −COOH group per MHA molecule), and Na^+ was from the ionization of NaOH (pH adjuster) in water. In view of the dynamics of reversible reactions, of which the above ion-paring reaction in the aqueous phase is one (Scheme 1, Phase (i)), the CTA^+ bound $Au_{25}(MHA)_{18}$ NCs (hereafter referred to as $Au_{25}(MHA)_{18}$@*x*CTA where *x* is the number of CTA^+ per NC) should initially contain a range of *x* values. It is reasonable to expect that $Au_{25}(MHA)_{18}$@*x*CTA NCs with *x* exceeding certain threshold values are sufficiently hydrophobic to be selectively extracted from the aqueous phase to the organic phase (Scheme 1, Phase (ii));[54,55] and the ion-pairing reaction would reform the departed species in the aqueous phase in order to restore equilibrium. We term such regenerative mechanism as "phase-transfer (PT) driven ion-pairing" (Scheme 1). Since the PT is driven by the affinity of $Au_{25}(MHA)_{18}$@*x*CTA NCs for the organic medium, it will be the most effective when there is a match of polarities between the NCs and the medium. Consequently, a deliberate control of the organic medium polarity should allow $Au_{25}(MHA)_{18}$@*x*CTA NCs with the desired polarity (or specific *x* values) to be selectively extracted from the aqueous phase. In particular, $Au_{25}(MHA)_{18}$@*x*CTA NCs with good amphiphilicity and moderate polarity imparted by an intermediate *x* value (e.g., *x* = ∼9) should be easily extracted by a *moderately polar* organic medium to support the volume production of NC amphiphiles by the PT driven ion-pairing mechanism. The following is a detailed account of the experimental demonstration of this hypothesis.

The synthesis of $Au_{25}(MHA)_{18}$ NCs was based on a previous procedure with some minor changes.[17] The raw $Au_{25}(MHA)_{18}$ NC aqueous solution prepared as such was brown in color (inset **#1** in Figure 1a) and showed the absorption characteristics of pure $Au_{25}(SR)_{18}$ NCs at 440 and 672 nm (Figure 1a, black line). The well-defined absorption spectrum is an indication of the high quality of the $Au_{25}(MHA)_{18}$ NCs in the raw product. The quality of $Au_{25}(MHA)_{18}$ NCs was confirmed by electrospray-ionization mass spectrometry (ESI-MS). In the broad *m*/*z* range of 1000−4000, two clusters of peaks were found at around *m*/*z* = 1280 and 1540 (Figure 1b) in good agreement with ionized NCs with 6− and 5− charges, respectively. The detailed assignment of the ESI-MS spectrum of ionized NCs with 5− charge is shown in the insets of Figure 1b as an example.

Amphiphilic Au_{25} NCs were prepared by the PT driven ion-paring reaction between CTA^+ and $-COO^-$ on the surface of $Au_{25}(MHA)_{18}$ NCs. A *moderately polar* ethanol/toluene mixture was the organic medium used to extract amphiphilic Au_{25} NCs selectively from the aqueous phase. Experimentally, calculated amounts of cetyltrimethylammonium bromide (CTAB) and $Au_{25}(MHA)_{18}$ NCs (in a CTAB:Au mole ratio of 100:1) were mixed in a mixed solvent system consisting of an equal volume of water, ethanol, and toluene. The partition of ethanol between water and toluene led to the formation of an organic phase containing ethanol and toluene. The mixture was stirred for 5 min and then kept still for 10 min. The Au_{25} NCs were completely transferred from the aqueous phase to the organic

DOI: 10.1021/jacs.5b00090
J. Am. Chem. Soc. 2015, 137, 2128−2136

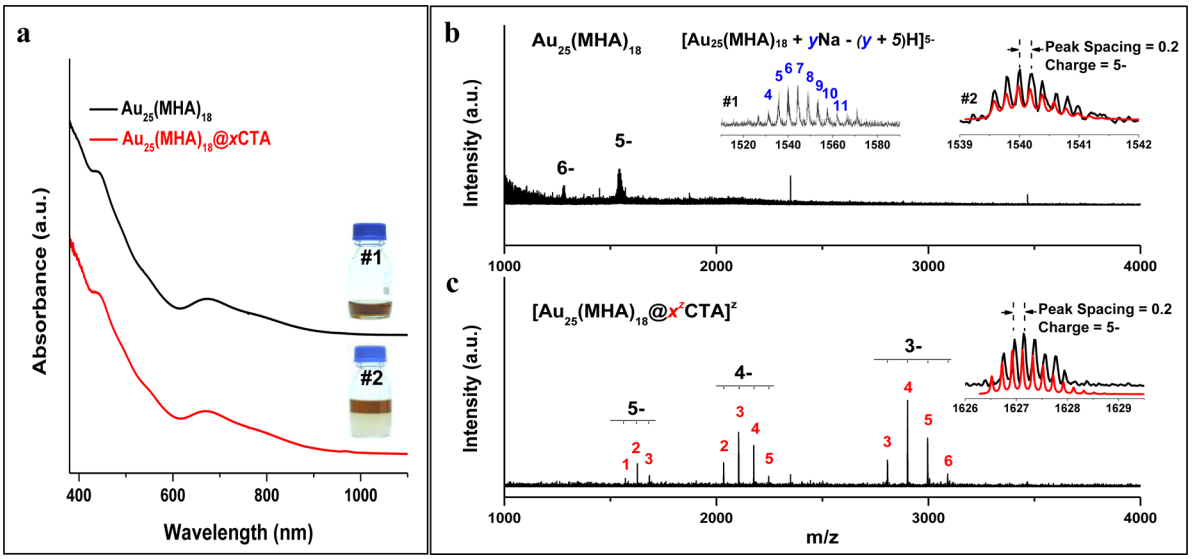

Figure 1. (a) UV−vis absorption spectra of $Au_{25}(MHA)_{18}$ (black line) and phase-transferred $Au_{25}(MHA)_{18}$@*x*CTA (red line) NCs; the insets in (a) are the digital photos of freshly prepared $Au_{25}(MHA)_{18}$ NCs in aqueous solution (**#1**) and the phase-transferred $Au_{25}(MHA)_{18}$@*x*CTA NCs in the organic phase (**#2**). (b) ESI-MS spectrum of $Au_{25}(MHA)_{18}$ NCs in the negative-ion mode. The charges on the ionized NC species are shown above each set of peaks; inset **#1** in (b) is the zoomed-in spectrum of ionized $Au_{25}(MHA)_{18}$ NCs with 5− charge, with the number of coordinated Na^+ shown above each peak; inset **#2** in (b) shows the experimental (black line) and simulated (red line) isotope patterns of $[Au_{25}(MHA)_{18} + 6Na - 11H]^{5-}$. (c) Negative-ion ESI-MS spectrum of phase-transferred $Au_{25}(MHA)_{18}$@*x*CTA NCs, with the value of x^z (the apparent number of CTA^+ in each NC with charge *z*) shown in red above each peak; the inset in (c) is the experimental (black line) and simulated (red line) isotope patterns of $[Au_{25}(MHA)_{18}$@2CTA − $7H]^{5-}$.

phase (inset **#2** in Figure 1a), indicating the successful binding of CTA^+ ions to the surface of $Au_{25}(MHA)_{18}$ NCs by this procedure. UV−vis spectroscopy was first used to examine the core size of the phase-transferred NCs (denoted as PT-NCs). The resulting spectrum, which is reproduced in Figure 1a (red line), was almost identical to the spectrum of the $Au_{25}(MHA)_{18}$ NCs before PT. Hence, the CTA^+ binding did not alter the core structure of the original $Au_{25}(MHA)_{18}$ NCs.

ESI-MS (in the negative-ion mode) was then used to examine the extent of CTA^+ binding on PT-NCs, i.e., the *x* value in $Au_{25}(MHA)_{18}$@*x*CTA NCs. The ESI-MS spectrum of PT-NCs in Figure 1c shows three sets of intense peaks in the broad *m*/*z* range of 1000−4000. They could be assigned to ionized $Au_{25}(MHA)_{18}$@*x*CTA NCs with 5− (*m*/*z* = ∼1627), 4− (*m*/*z* = ∼2105), and 3− (*m*/*z* = ∼2902) charge, respectively. A representative isotope analysis of $[Au_{25}(MHA)_{18}$@2CTA − $7H]^{5-}$ is shown in the inset of Figure 1c. The apparent number of CTA^+ in each ionized NC species carrying a charge of *z* (referred as x^z) is also labeled in the ESI-MS spectrum (Figure 1c) for easy identification. It can be seen that the species with 3− charge (the cluster of peaks at *m*/*z* = ∼2902) consisted of a distribution of x^{3-} from 3 to 6 (with a population maximum at 4), while the distributions of x^{4-} and x^{5-} contained mostly x^{4-} = 2−5 (population maximum at 3) and x^{5-} = 1−3 (population maximum at 2), respectively. Despite the variations in peak intensity, the outlines enveloping the peaks of NC species with 3−, 4−, and 5− charge were visually similar, and the corresponding peak intensities were found to follow the approximate relation of $x^{3-} \sim x^{4-} + 1 \sim x^{5-} + 2$ (e.g., using the x^{z-} values of the most prominent peaks for the 3−, 4−, and 5− species, x^{3-} (= 4) = x^{4-} (= 3) +1 = x^{5-} (=2) + 2). This suggests that the development of negative charge in these ionized NCs was most likely based on the successive dissociation of CTA^+ from the Au NCs. The observation of the dissociation of bulky hydrophobic cations before smaller cations (e.g., H^+) in ESI has previously been reported by Lee et al.[24] On this basis, the total number of CTA^+ in the neutral form of $Au_{25}(MHA)_{18}$@*x*CTA NC (i.e., *x*) may be calculated as follows:

$$x = x^z - z \tag{2}$$

Therefore, we inferred that there were 6−9 (with a population maximum at 7) CTA^+ per $Au_{25}(MHA)_{18}$ NC in the charge-neural PT-NCs. Given that each $Au_{25}(MHA)_{18}$ NC contains 18 hydrophilic MHA ligands and the 1:1 pairing between MHA and CTA^+, the 6−9 CTA^+ per NC would correspond to approximately half of a monolayer coverage of hydrophobic moieties on the $Au_{25}(MHA)_{18}$ NC surface. This implies that $Au_{25}(MHA)_{18}$@*x*CTA NCs (*x* = 6−9) were protected by a comparable number of hydrophilic MHA and hydrophobic CTA^+−MHA paired ligands (i.e., MHA···CTA where hydrophobicity is imparted by the hydrocarbon ends of CTA^+). It also shows that amphiphilic NCs could be formed in high yield by the PT driven ion-pairing reaction using a *moderately polar* ethanol/toluene mixture as the organic extractant.

Several control experiments were used to verify the formation of $Au_{25}(MHA)_{18}$@*x*CTA NCs (*x* = 6−9) via the proposed polarity-dependent PT driven ion-pairing mechanism. First, we disabled the PT of Au_{25} NCs by tuning the polarity of the organic phase to highly nonpolar (CTAB has low solubility in a nonpolar solvent such as toluene). As shown in the inset of Figure 2a(i), the $Au_{25}(MHA)_{18}$@*x*CTA NCs could not migrate to the organic phase from the aqueous phase when ethanol was eliminated from the trisolvent system (volume fraction of ethanol, f_{EtOH} = 0). Without the transfer of the NC species to the organic phases, the ion-pairing reaction occurred to the full extent allowable by thermodynamics in the aqueous solution. The non-phase-transferred product formed as such was $Au_{25}(MHA)_{18}$@*x*CTA NCs (*x* = 3−5, referred to henceforth as non-PT-NCs). The *x* value was calculated based on the x^{3-} species in Figure 2b(i) according to eq 2. These non-PT-NCs (*x* = 3−5) were much

DOI: 10.1021/jacs.5b00090
J. Am. Chem. Soc. 2015, 137, 2128−2136

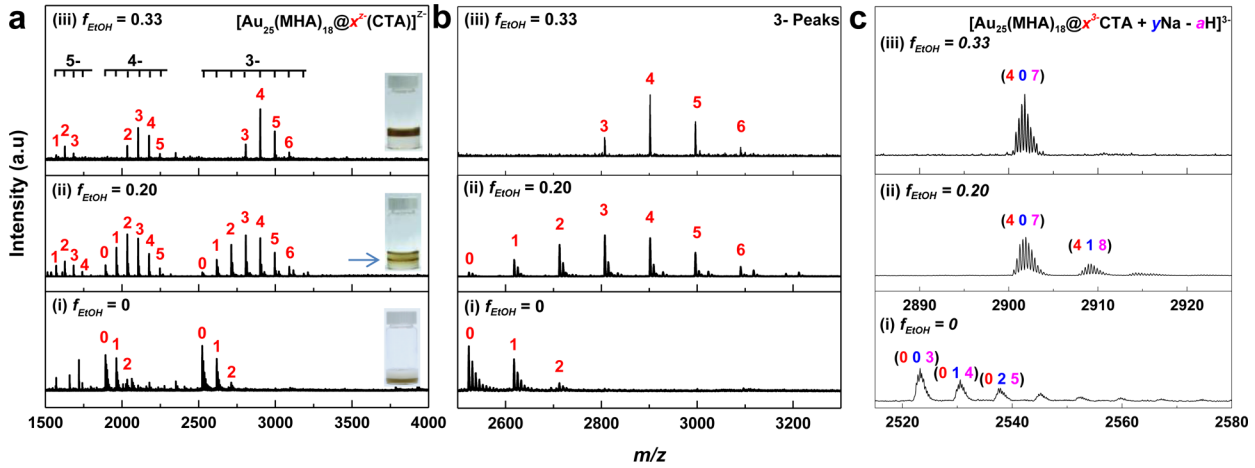

Figure 2. Comparison of the ESI-MS spectra (in negative-ion mode) of non-phase-transferred (i), intermediate-phase-transferred (ii), and phase-transferred (iii) $Au_{25}(MHA)_{18}@x$CTA NCs prepared with f_{EtOH} = 0, 0.20, and 0.33, respectively. (a) Spectra in the broad 1500−4000 m/z region; the insets in (a) show corresponding digital photos of $Au_{25}(MHA)_{18}@x$CTA NCs, where the blue arrow in (ii) indicates the intermediate-phase-transferred $Au_{25}(MHA)_{18}@x$CTA NCs agglomerating at the aqueous−organic interface. (b) Zoomed-in spectra of NC species with 3− charge. (c) Zoomed-in spectra of representative peaks in (b).

more hydrophilic than the PT-NCs (x = 6−9, obtained with f_{EtOH} = 0.33, the ESI-MS spectra of which are also included in Figure 2, panel (iii) for ease of comparison). The formation of these more hydrophilic (i.e., smaller x values) non-PT-NCs could be attributed to the presence of excess Na^+ in the aqueous phase, which shifted the ion-pairing equilibrium (eq 1) significantly to the left and, consequently, a smaller extent of CTA^+ binding on the $Au_{25}(MHA)_{18}$ NC surface. This hypothesis is supported by a series of peaks due to Na^+ coordination in the ESI-MS spectrum of non-PT-NCs (Figure 2c(i)). There was no similar series of peaks in the ESI-MS spectrum of PT-NCs (Figure 2c(iii)).

Using a solvent mixture with an intermediate f_{EtOH} value of 0.20, we were able to control the PT to the extent that $Au_{25}(MHA)_{18}@x$CTA NCs were agglomerated at the aqueous−organic interface (inset of Figure 2a(ii)). These NCs may be referred to as intermediate-PT-NCs. Since the intermediate-PT-NCs were in contact with both aqueous and organic phases, they acquired the surface features of non-PT-NCs and PT-NCs. This is evidenced from the broad distribution of x values (x = 3−9) in their ESI spectrum. The x values were calculated based on the x^{3-} species in Figure 2b(ii) according to eq 2. Peaks due to some slight Na^+ coordination were detected in the ESI-MS spectrum of intermediate-PT-NCs (Figure 2c(ii)). All of these observations are consistent with the proposed PT driven ion-pairing mechanism, where polarity-dependent selective PT of certain NC species (e.g., $Au_{25}(MHA)_{18}@x$CTA NCs (x = 6−9), obtained by using a *moderately polar* ethanol/toluene mixture) could drive the ion-pairing reaction to sustain the formation of the extracted NC species. Additional details about the ESI-MS spectra (including the wide-scan spectra and representative isotope analyses) of non-PT-NCs, intermediate-PT-NCs, and PT-NCs can be found in Figure 2a and Figure S1 (in the Supporting Information).

As an important corollary of the polarity-dependent PT driven ion-pairing, Au NCs with a more hydrophobic surface should be producible by the PT of NCs into a low polarity organic solvent. We verified this corollary by carrying out the PT driven ion-pairing reaction using pure toluene as the extraction medium. In this case, a bulkier and more hydrophobic cation, tetraoctylammonium (TOA^+), was used in lieu of CTA^+ to enable the PT. UV−vis analysis (Figure S2a) confirmed the conservation of the Au_{25} core structure in these phase-transferred NCs (referred to as $Au_{25}(MHA)_{18}@x$TOA NCs). ESI-MS analysis (Figure S2b-d) suggested x = 8−11 in $Au_{25}(MHA)_{18}@x$TOA NCs, higher than that in the case of $Au_{25}(MHA)_{18}@x$CTA NCs (x = 6−9). A greater extent of hydrophobic cation binding, together with the more hydrophobic nature of TOA^+, rendered the surface of the NCs to be hydrophobic enough for selective extraction by a low polarity solvent (toluene).

Amphiphilicity of $Au_{25}(MHA)_{18}@x$CTA NCs (x = 6−9). The coexistence of hydrophilic MHA and hydrophobic MHA···CTA ligands in comparable amounts on the NC surface, and the flexible chain structure of these ligands, should make PT-NCs (i.e., $Au_{25}(MHA)_{18}@x$CTA, where x = 6−9) a potential NC amphiphile. Given that the sizes of the Au core, MHA ligands, and CTA^+ cations are quite comparable (~1.0,[6,56] 0.7, and 2.0 nm, respectively; see the illustration in Scheme 2), the polarity of

Scheme 2. Schematic Illustration of the Sizes of the Au Core, MHA, and CTA^+ Cations in $Au_{25}(MHA)_{18}@x$CTA NCs (x = 6−9)[a]

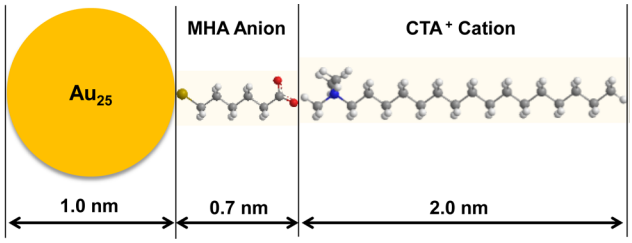

[a]The size of the Au_{25} core is taken from the literature,[6,56] and the lengths of MHA and CTA^+ are estimated by CS ChemOffice Ultra 4.5.

$Au_{25}(MHA)_{18}@x$CTA (x = 6−9) NCs should depend on the way MHA and MHA···CTA ligands are arranged on the NC surface. The flexible hydrocarbon chains of MHA (C_6-chain) and CTA^+ (C_{16}-chain) enable these ligands to easily organize into different configurations on the $Au_{25}(MHA)_{18}@x$CTA NCs (x = 6−9) to adapt to the solvent polarity. For example, in a polar environment, the hydrophobic MHA···CTA ligands could bunch together at one end of the NC to leave the hydrophilic MHA

DOI: 10.1021/jacs.5b00090
J. Am. Chem. Soc. 2015, 137, 2128−2136

Scheme 3. Schematic Illustration of the Self-Assembly Process of PT-NCs ($Au_{25}(MHA)_{18}$@xCTA NCs where x = 6−9))

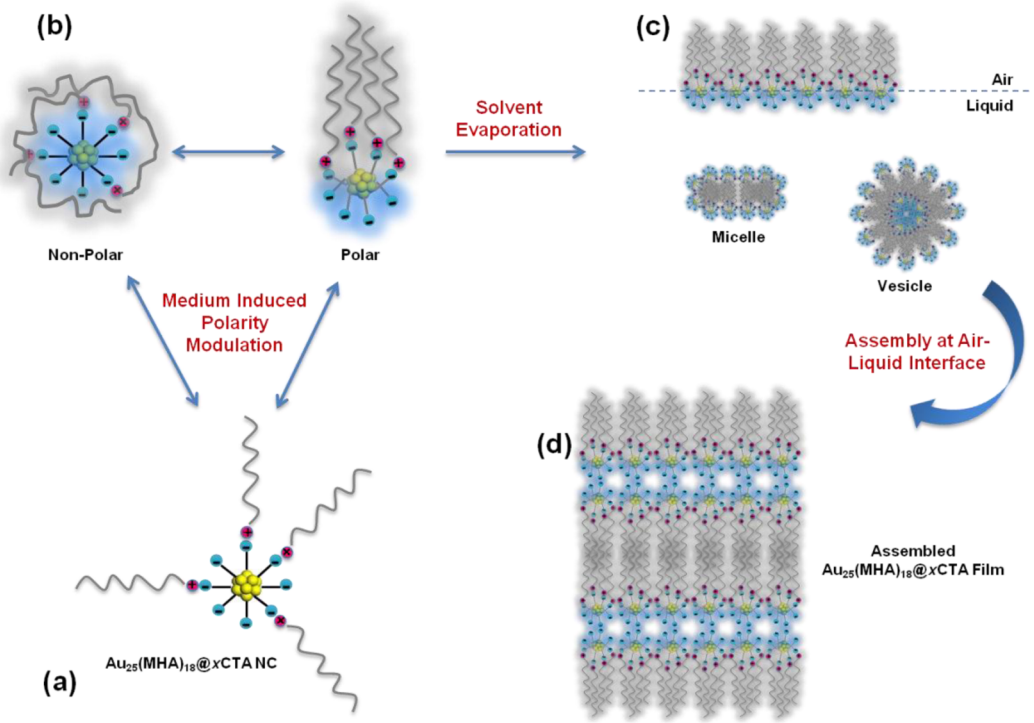

ligands exposed at the opposite end to maximize the NC polarity (the polar configuration illustrated in Scheme 3b). On the contrary, the hydrophobic MHA···CTA ligands could also fold over on top of the hydrophilic MHA ligands to minimize the polarity of NCs in a nonpolar environment (the nonpolar configuration illustrated in Scheme 3b). Such a medium-induced polarity modulation mechanism could maximize amphiphilicity by adapting the surface of $Au_{25}(MHA)_{18}$@xCTA NCs (x = 6−9) to the environment (a "smart" surface of sorts).

The amphiphilic character of $Au_{25}(MHA)_{18}$@xCTA NCs (x = 6−9) was first demonstrated by their good solubility in solvents with very different polarities. The polarity of a solvent is usually measured by its relative dielectric constant, ε_r. The purified $Au_{25}(MHA)_{18}$@xCTA NCs (x = 6−9) could form homogeneous solutions in mixed solvents covering a wide range of ε_r values from 4.15 (ethanol/hexane =10/90 v/v) to 41.25 (ethanol/water =70/30 v/v). These NC solutions (with NC concentration [NC] = 0.02 mM) were clear (insets of Figure 3a) and stable to mechanical disturbance. Centrifugation at 10,000 rpm for 10 min did not result in any precipitation, as shown by the superimposable UV−vis absorption spectra of the NC solution before and after centrifugation (Figure 3a). Transmission electron microscopy (TEM) images (Figure 3b−f) of $Au_{25}(MHA)_{18}$@xCTA NCs (x = 6−9) confirm their good dispersibility in the solution. No nanoparticles or aggregates larger than 3 nm were found in the TEM images. The high resolution TEM (HR-TEM) images (Figure 3b−f insets) also confirm the smallness (<2 nm) and the discreteness of the $Au_{25}(MHA)_{18}$@xCTA NCs (x = 6−9) in these media. To the best of our knowledge, the $Au_{25}(MHA)_{18}$@xCTA NC (x = 6−9) in this study could be the NC family with the broadest medium polarity window where homogeneous NC solutions may form. A ε_r outside of the aforementioned window would render the $Au_{25}(MHA)_{18}$@xCTA NC (x = 6−9) difficult or unable to dissolve. For example, dimethyl sulfoxide (DMSO, ε_r = 46.70) and hexane (ε_r = 1.88) were respectively the nonsolvent and the poor solvent for $Au_{25}(MHA)_{18}$@xCTA NCs (x = 6−9).

Self-Assembly of Amphiphilic $Au_{25}(MHA)_{18}$@xCTA NCs (x = 6−9). A remarkable feature of molecular amphiphiles is the formation of bilayers and lamellar structures (e.g., lyotropic liquid crystals) by self-assembly.[52,57] Likewise our NC analog of molecular amphiphiles also exhibited self-assembly properties. The investigation of the self-assembly characteristics of $Au_{25}(MHA)_{18}$@xCTA NCs (x = 6−9) was carried out in a DMSO/ethanol mixture (50/50 v/v), where volatile ethanol is a good solvent for $Au_{25}(MHA)_{18}$@xCTA NCs (x = 6−9) and nonvolatile DMSO is a poor solvent. The preferential evaporation of ethanol could therefore induce the self-assembly of $Au_{25}(MHA)_{18}$@xCTA NCs (x = 6−9) at the air−liquid interface. Experimentally, purified $Au_{25}(MHA)_{18}$@xCTA NCs (x = 6−9) were redissolved in a DMSO/ethanol mixture (50/50 v/v) to a [NC] of 0.53 mM. Solvent evaporation was carried out at ambient conditions (298 K and 1 atm) over a period of 2−3 days. A brownish-black film (inset **#2** in Figure 4a) was formed at the air−liquid interface by the end of the procedure.

The brownish-black film was first characterized by UV−vis absorption spectroscopy. The film was redissolvable in ethanol and the ethanol solution of the film was indistinguishable from the ethanol solution of $Au_{25}(MHA)_{18}$@xCTA NCs (x = 6−9) (Figure 1a, red line) by UV−vis absorption spectroscopy (Figure 4a). This is possible if the brownish-black film was an organized aggregate of the $Au_{25}(MHA)_{18}$@xCTA NCs (x = 6−9). The morphology of these film-like $Au_{25}(MHA)_{18}$@xCTA NCs (x = 6−9) was then examined by field-emission scanning electron microscopy (FESEM). The FESEM images (Figure 4b and c) show a deformable (evidenced by the presence of creases in Figure 4b) flexible sheet-like structure with a typical thickness of ~15 nm (see high resolution FESEM image in Figure 4c). The X-ray diffraction (XRD) pattern of the film (Figure 4d) contains two distinctive diffraction peaks at 2θ = 4.02° and 7.08°. The

DOI: 10.1021/jacs.5b00090
J. Am. Chem. Soc. 2015, 137, 2128−2136

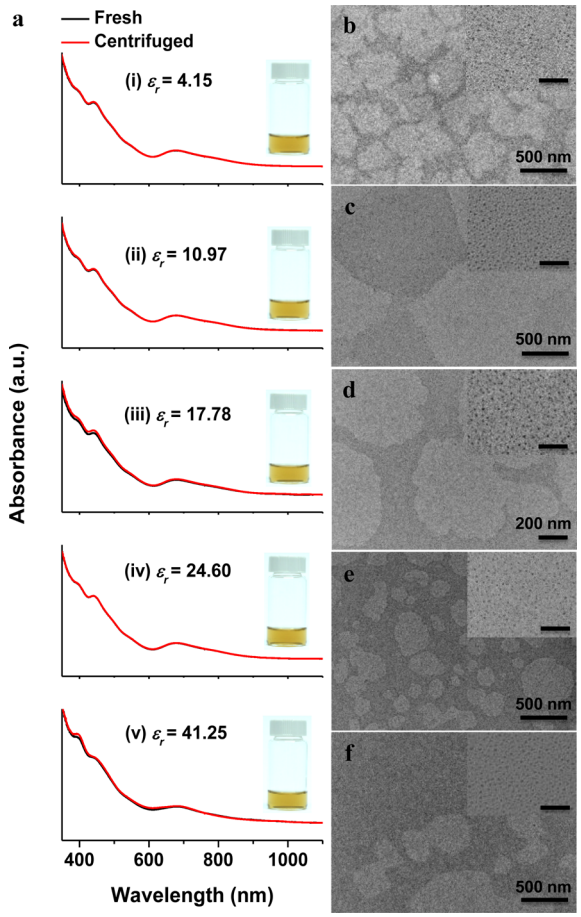

Figure 3. (a) UV−vis absorption spectra and (b−f) TEM images of $Au_{25}(MHA)_{18}$@xCTA NCs (x = 6−9) in different media: (a(i), b) ethanol/hexane = 10/90 v/v, ε_r = 4.15; (a(ii), c) ethanol/hexane = 40/60 v/v, ε_r = 10.97; (a(iii), d) ethanol/hexane = 70/30 v/v, ε_r = 17.78; (a(iv), e) ethanol, ε_r = 24.60; and (a(v), f) ethanol/water = 70/30 v/v, ε_r = 41.25. The superimposed black and red lines in (a) are respectively the UV−vis absorption spectra of freshly prepared and centrifuged (at 10,000 rpm for 10 min) NC solutions. The insets in (a) are the digital images of freshly prepared NC solutions. The insets in (b−f) are corresponding high resolution TEM images of the NCs, where the scale bars are 20 nm. All measurements were taken at [NC] = 0.02 mM.

bimodal XRD pattern is typical of the formation of regularly stacked bilayer structures where there are two characteristic interlayer distances (d) corresponding to the hydrophilic and hydrophobic zones respectively (see schematic illustration in the inset of Figure 4d and Scheme 3d). Hence the sheet-like structure in the FESEM images (Figure 4b and c) most probably consisted of ordered stacking of bilayers of $Au_{25}(MHA)_{18}$@xCTA NCs (x = 6−9). Since the thickness of the sheet-like structure (~15 nm) was much larger than the size of a $Au_{25}(MHA)_{18}$@xCTA NC (x = 6−9) (see Scheme 2 for a schematic illustration), the thin film was $Au_{25}(MHA)_{18}$@xCTA NCs (x = 6−9) stacked to resemble a lamellar bilayer structure formed by molecular amphiphiles.

The layered structure of these $Au_{25}(MHA)_{18}$@xCTA NC films (x = 6−9) was also confirmed by TEM analysis (Figure 4e and f). We managed to exfoliate a film in DMSO through a brief ultrasonication (37 kHz, 5 min). A droplet of the resultant DMSO solution was drop-cast on a TEM copper grid and dried. The TEM image shows a single-NC-thick sheet which was folded in several places (Figure 4e). The HR-TEM image (Figure 4f) confirms the sheet was composed of small NCs (<2 nm). There was however no indication of the intralayer structural order in each NC layer (Figure 4f), verifying that the XRD peaks were caused by diffraction from regular interlayer distances.

The stacked bilayer structure could be formed by the aggregation and rearrangement of micelles or vesicles of amphiphilic $Au_{25}(MHA)_{18}$@xCTA NCs (x = 6−9) at the air−liquid interface. With the evaporation of ethanol, the polarity of the DMSO/ethanol mixture gradually increased. In the early stages of evaporation, the "smart" surface of $Au_{25}(MHA)_{18}$@xCTA NCs (x = 6−9) was able to undergo rearrangement to adapt to the changing polarity of the medium and kept them soluble in the mixed solvent. However, continual evaporation of ethanol would eventually increase the polarity of the DMSO/ethanol mixture to exceed the upper polarity limit of the NCs, resulting in the precipitation of $Au_{25}(MHA)_{18}$@xCTA NCs (x = 6−9) in their most polar configuration (surfactant-like or polar configuration in Scheme 3b).

The aggregation habit of these precipitated surfactant-like NCs at the air−liquid interface was different from that in the bulk of the liquid, due to the difference in surface ("interfacial") energies. As illustrated in Scheme 3c, at the air−liquid interface, the surfactant-like NCs self-assembled into a monolayer with the hydrophobic end facing air, similar to the behavior of a molecular surfactant at the air−liquid interface. In the bulk of the liquid (DMSO-rich), the surfactant-like NCs aggregated into micelles or vesicles with their hydrophilic ends facing the DMSO-rich environment (Scheme 3c). The formation of these secondary structures in the bulk liquid was confirmed by dynamic light scattering (DLS) analysis, where a significant increase in hydrodynamic diameter (from ~5.0 to 459.6 nm) was observed after 1 day of evaporation (Figure S3). These NC micelles or vesicles then migrated to the air−liquid interface and adhered to the monolayer of surfactant-like NCs via hydrophilic−hydrophilic interaction. As a result of the maximization of the hydrophilic−hydrophilic interaction and minimization of surface energy, these NC micelles or vesicles would rearrange into stacks of bilayers on the previously formed monolayer of NCs, in order to allow the hydrophilic ends to be in contact with the hydrophilic ends of the NC monolayer and the bulk of the liquid phase. A succession of these hydrophilic−hydrophilic induced adhesions and rearrangements would stack the bilayers into the ~15-nm-thick sheet-like structure (Scheme 3d). However, it should be mentioned that this is only a hypothesis; a molecular level understanding of the rearrangement mechanism is not available at the current stage of research.

In the above self-assembly of bilayers, the d-spacing corresponding to the hydrophobic−hydrophobic and hydrophilic−hydrophilic zones could be estimated based on the size of the Au core (~1.0 nm), the MHA ligands (~0.7 nm), and the CTA^+ (~2.0 nm, see Scheme 2). In the fully extended forms of the MHA ligands and CTA^+ (Au core is considered impenetrable and undeformable), the d values corresponding to hydrophilic−hydrophilic and hydrophobic−hydrophobic zones should be 2.4 (=1.0 + 2 × 0.7) and 6.4 (=1.0 + 2 × (2.0 + 0.7)) nm, respectively. These estimated d values are in good agreement with those measured by XRD (Figure 4d). If we consider 2θ = 4.02° and 7.08° peaks as second order diffraction peaks (the first order diffraction peaks were overshadowed by the high background noise at 2θ < 2.5°), the second order diffraction at 2θ = 7.08° should correspond to a d value of 2.5 nm, close to the value of the hydrophilic zone (estimated d = 2.4 nm) formed by fully extended MHA ligands. The d value corresponding to the

DOI: 10.1021/jacs.5b00090
J. Am. Chem. Soc. 2015, 137, 2128−2136

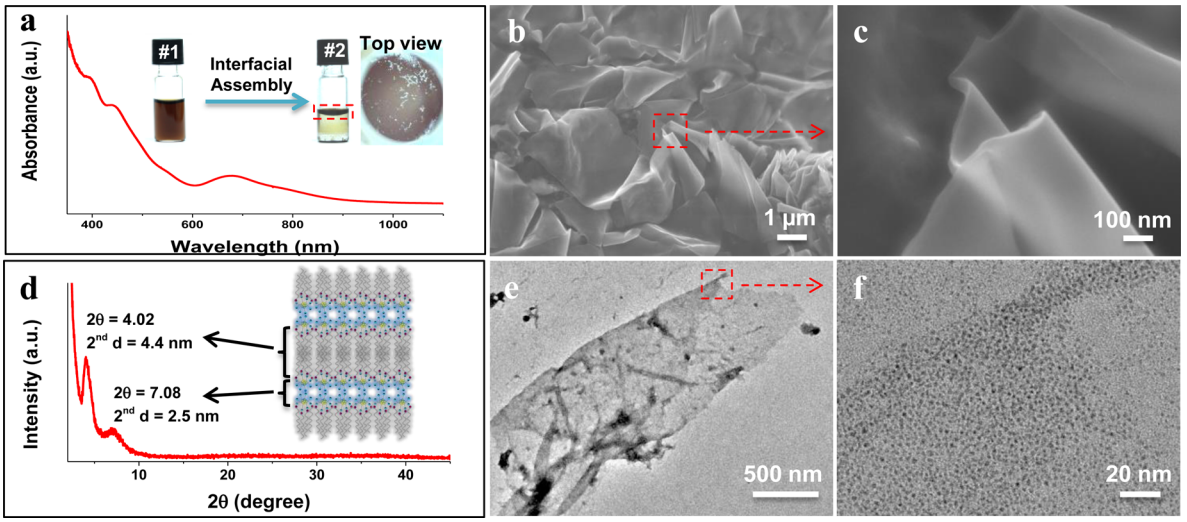

Figure 4. (a) UV−vis absorption spectrum, (b and c) FESEM images, (d) XRD pattern, and (e and f) TEM images of PT-NCs $(Au_{25}(MHA)_{18}@xCTA$ NCs where $x = 6–9)$ assembled at the air−liquid interface. The insets in (a) are the digital photos of $Au_{25}(MHA)_{18}@xCTA$ NCs before (**#1**) and after (**#2**) self-assembly; the top view of the boxed area of **#2** is also shown to the right of **#2**. The inset in (d) shows a schematic illustration of the sheet-like assembly formed by the NC bilayers.

second order diffraction at $2\theta = 4.02°$ is 4.4 nm, smaller than the estimated value (d = 6.4 nm) of the hydrophobic zone. This could be due to some interdigitation of the hydrocarbon tails of CTA^+. The interdigitation of the long alkyl-chain of CTA^+ in bilayer formation is a rather common phenomenon.[58−61] Based on the above XRD analysis, the number of bilayers in the ~15-nm-thick sheet-like structure was ~2 (i.e., 15/(4.4 + 2.5) = 2.17).

Enhanced Stability of $Au_{25}(MHA)_{18}@xCTA$ NCs (x = 6–9). In addition to imparting amphiphilicity, the CTA^+ coating also contributed to improving the stability of Au_{25} NCs. This was revealed by comparing the stability of $Au_{25}(MHA)_{18}$ NCs and $Au_{25}(MHA)_{18}@xCTA$ NCs (x = 6–9) at ambient conditions (298 K, 1 atm and mildly oxidizing due to the oxygen in air) over a period of 7 days. NC stability was inferred from the spectral changes in UV−vis spectroscopy (Figure 5). The UV−vis absorption spectrum of $Au_{25}(MHA)_{18}$ NCs after 3 days of aging showed considerable changes indicating the deterioration in NC quality (Figure 5a). In sharp contrast, the UV−vis absorption spectrum of $Au_{25}(MHA)_{18}@xCTA$ NCs (x = 6–9) (Figure 5b) underwent very little changes even over a much longer period of time (7 days). Good stability was also observed for the stacked $Au_{25}(MHA)_{18}@xCTA$ NC (x = 6–9) bilayers. The stability of the latter was evaluated at elevated temperature (393 K) in air and in vacuum for 3 days. The assembled film after the said thermal treatment was redissolved in ethanol for the UV−vis absorption analysis. The results in Figure S4 show that the characteristic absorption features of $Au_{25}(SR)_{18}$ NCs at 440 and 672 nm were still present in both cases, and hence the assembled $Au_{25}(MHA)_{18}@xCTA$ NCs (x = 6–9) were stable to high temperature (373 K) even in air. These stability tests suggest that the CTA^+ coating was an effective O_2 barrier to protect the Au_{25} core from oxidation (a common degradation pathway for Au_{25} NCs).[62,63] It might also increase the thermal stability of the NCs by dispersing the applied thermal energy through vibrations or rotations of the C_{16}-chains, without which thermal desorption of the thiolate ligands would occur to cause the aggregation of the Au cores.

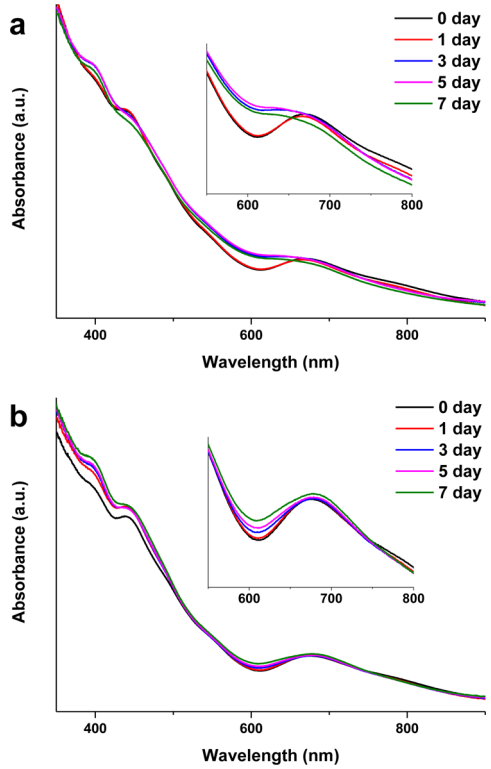

Figure 5. UV−vis spectra of (a) $Au_{25}(MHA)_{18}$ NCs and (b) $Au_{25}(MHA)_{18}@xCTA$ NCs (x = 6–9) over a period of 1 week at the ambient conditions (298 K and 1 atm). The insets show the enlarged spectra in the 550−800 nm spectral region. The absorption peak at ~672 nm of $Au_{25}(MHA)_{18}$ NCs was significantly broadened after 3 days, while the absorption peak of $Au_{25}(MHA)_{18}@xCTA$ NCs (x = 6–9) did not show noteworthy broadening over 7 days, indicating better stability of the latter. $Au_{25}(MHA)_{18}$ NCs were dissolved in ultrapure water, and $Au_{25}(MHA)_{18}@xCTA$ NCs (x = 6–9) were dissolved in ethanol.

CONCLUSION

In summary, we have developed a simple surface modification method enabling the preparation of amphiphilic noble metal

DOI: 10.1021/jacs.5b00090
J. Am. Chem. Soc. 2015, 137, 2128−2136

NCs. The method is based on a PT driven ion-pairing reaction between hydrophobic cations and the anionic surface functionality of the hydrophilic NCs. The reversibility of the ion-pairing reaction combined with a polarity-dependent PT enables amphiphilic NCs to be extracted selectively from the aqueous phase to a *moderately polar* organic phase, thereby making the preparation of amphiphilic NCs possible. Specifically, amphiphilic $Au_{25}(MHA)_{18}$@*x*CTA NCs (x = 6−9) were formed by patching the surface of hydrophilic $Au_{25}(MHA)_{18}$ NCs partially with CTA^+ leveraging on the hydrocarbon chain of the latter to provide hydrophobicity. Due to the presence of a comparable amount of flexible hydrophilic and hydrophobic moieties on the NC surface, the resulting amphiphilic $Au_{25}(MHA)_{18}$@*x*CTA NCs (x = 6−9) not only acquired good solubility in a wide range of solvents with distinctly different polarities (ε_r ranging from 4.15 to 41.25) but also mirrored the self-assembly characteristics of molecular amphiphiles (e.g., formation of stacked bilayers with *regular* interlayer packing at the air−liquid interface). The products and the preparation method demonstrated in this study indicate that amphiphilicity can now be imparted to sub-2-nm particles to increase the versatility of NC-based materials and to regulate the self-assembled structures of the latter.

EXPERIMENTAL SECTION

Materials and Instruments. Hydrogen tetrachloroaurate(III) trihydrate ($HAuCl_4{\cdot}3H_2O$), 6-mercaptohexanoic acid (MHA), cetyltrimethylammonium bromide (CTAB), and sodium borohydride ($NaBH_4$) from Sigma-Aldrich; acetone, acetonitrile, dichloromethane (CH_2Cl_2), and sodium hydroxide (NaOH) from Merck; tetraoctylammonium bromide (TOAB) from Alfa Aesar; ethanol (EtOH) and hexane from Fisher; methanol (MeOH) from J. T. Baker and dimethyl sulfoxide (DMSO) from Tedia; were all used as received. All aqueous solutions were prepared in Ultrapure Millipore water (18.2 MΩ). All glassware were washed with *aqua regia* and rinsed with ethanol and ultrapure water before use.

UV−vis absorption spectra were recorded by a Shimadzu UV-1800 spectrometer. The molecular formulas of Au_{25} NCs were deduced by electrospray ionization mass spectrometry (ESI-MS) on a Bruker microTOF-Q system operating in a negative-ion mode. The ESI-MS samples of $Au_{25}(MHA)_{18}$ and non-phase-transferred $Au_{25}(MHA)_{18}$@*x*CTA NCs were prepared in ultrapure water, while those of intermediate-phase-transferred and phase-transferred $Au_{25}(MHA)_{18}$@*x*CTA and $Au_{25}(MHA)_{18}$@*x*TOA NCs were prepared in an acetonitrile/methanol mixture (75/25 v/v). The XRD pattern of assembled $Au_{25}(MHA)_{18}$@*x*CTA NCs (x = 6−9) was recorded by a Bruker D8 advance X-ray diffractometer using a Cu K_α source (λ = 1.5405 Å). Transmission electron microscopy (TEM) and field-emission scanning electron microscopy (FESEM) were performed on a JEOL JEM 2010 microscope operating at 200 kV, and a JEOL JSM-6700F microscope operating at 5 kV, respectively. TEM and FESEM samples of the solution product were typically prepared by dispensing a drop of the solution onto a copper grid, followed by overnight drying at the ambient condition (298 K and 1 atm). The FESEM sample of the assembled film was prepared by slicing a piece of film from the air−liquid interface, followed by drying in a Binder VD-23 vacuum oven (333 K and ∼20 mbar) overnight.

Synthesis of $Au_{25}(MHA)_{18}$ NCs. The synthesis of $Au_{25}(MHA)_{18}$ followed a reported procedure with several minor modifications.[17] Briefly, 29.7 mg MHA and 5 mL of 20 mM $HAuCl_4$ aqueous solution were mixed in 100 mL of ultrapure water to form yellowish Au(I)-MHA complexes. Four mL of 1 M NaOH aqueous solution was then added to bring the pH of the solution to ∼10, followed by the dropwise addition of 2 mL of 112 mM $NaBH_4$ in 0.2 M NaOH aqueous solution. After vigorously stirring (at 1,000 rpm) for 3 h, a brownish aqueous solution of $Au_{25}(MHA)_{18}$ NCs was collected as the raw product.

Synthesis of Phase-Transferred $Au_{25}(MHA)_{18}$@*x*CTA NCs. The raw product ($Au_{25}(MHA)_{18}$ NCs) was used for surface modification without further purification. 80 mL of the $Au_{25}(MHA)_{18}$ NC aqueous solution was mixed with 80 mL of 100 mM CTAB solution in ethanol under vigorous stirring (1,000 rpm), followed by the addition of 80 mL of toluene. The mixture was stirred for another 5 min, and then kept still for 10 min to allow the PT to complete. At the end of this procedure, phase-transferred $Au_{25}(MHA)_{18}$@*x*CTA NCs could be collected from the organic phase.

The raw phase-transferred $Au_{25}(MHA)_{18}$@*x*CTA NCs were precipitated by centrifugation (8,000 rpm, 5 min) after mixing with 2 equiv volume of hexane (i.e., 200 mL of hexane for every 100 mL of NC solution). The precipitate was recovered and washed by acetone-dichloromethane-dichloromethane-acetone (in sequence) to remove the residual CTAB and other impurities. The purified phase-transferred $Au_{25}(MHA)_{18}$@*x*CTA NCs were then dissolved in 2 mL of ethanol and kept for further use. ESI-MS analysis suggests x = 6−9 in the cleaned phase-transferred $Au_{25}(MHA)_{18}$@*x*CTA NCs (see Figure 1c and the corresponding text for details of ESI-MS analysis).

Synthesis of Intermediate-Phase-Transferred and Non-Phase-Transferred $Au_{25}(MHA)_{18}$@*x*CTA NCs. The intermediate-phase-transferred and non-phase-transferred $Au_{25}(MHA)_{18}$@*x*CTA NCs were similarly prepared; but with some revision of the amount of ethanol used in the synthesis. In the preparation of intermediate-phase-transferred $Au_{25}(MHA)_{18}$@*x*CTA NCs, 80 mL of $Au_{25}(MHA)_{18}$ NC aqueous solution was added with 40 mL of 200 mM CTAB ethanol solution (instead of 80 mL of 100 mM CTAB ethanol solution). In the preparation of non-phase-transferred $Au_{25}(MHA)_{18}$@*x*CTA NCs, 80 mL of $Au_{25}(MHA)_{18}$ NC aqueous solution was added in an amount equal to that of solid CTAB (8 mmol). The raw products of intermediate-phase-transferred and non-phase-transferred $Au_{25}(MHA)_{18}$@*x*CTA NCs were collected at the aqueous−organic interface and from the aqueous phase, respectively.

Synthesis of $Au_{25}(MHA)_{18}$@*x*TOA NCs (x = 8−11). The $Au_{25}(MHA)_{18}$@*x*TOA NCs were prepared via a procedure similar to that of $Au_{25}(MHA)_{18}$@*x*CTA NCs, except using the solid TOAB (8 mmol) instead of CTAB ethanol solution as hydrophobic salt source in the synthesis.

Self-Assembly of $Au_{25}(MHA)_{18}$@*x*CTA NCs (x = 6−9). The phase-transferred $Au_{25}(MHA)_{18}$@*x*CTA NCs (x = 6−9) after purification were dissolved in a DMSO/ethanol mixture (50/50 v/v) to a NC concentration ([NC]) of 0.53 mM. The solvent was then evaporated at the ambient conditions (298 K and 1 atm). The self-assembly was allowed to progress for 2−3 days. A brownish-black film was collected at the air−liquid interface as the self-assembly product.

ASSOCIATED CONTENT

Supporting Information

Figure S1, isotope patterns of $Au_{25}(MHA)_{18}$@*x*CTA NCs; Figure S2, UV−vis and ESI-MS spectra of $Au_{25}(MHA)_{18}$@*x*TOA NCs; Figure S3, digital photos and DLS analysis of $Au_{25}(MHA)_{18}$@*x*CTA NCs assembled over different time periods; Figure S4, UV−vis spectra of assembled $Au_{25}(MHA)_{18}$@*x*CTA NCs after heat treatment at 373 K for 3 days. This material is available free of charge via the Internet at http://pubs.acs.org.

AUTHOR INFORMATION

Corresponding Authors

*J.X. e-mail: chexiej@nus.edu.sg.

*J.Y.L. e-mail: cheleejy@nus.edu.sg.

Notes

The authors declare no competing financial interest.

ACKNOWLEDGMENTS

We thankfully acknowledge Huiyuan Qu, Sofia Salina, and Amanda Jia-Yi Tay from School of Chemical and Life Sciences, Singapore Polytechnic, for their experimental assistance. This work is financially supported by the Ministry of Education,

DOI: 10.1021/jacs.5b00090
J. Am. Chem. Soc. 2015, 137, 2128−2136

Singapore, under Grants R279-000-349-112 and R279-000-409-112. Q.Y. acknowledges the National University of Singapore for his research scholarship.

REFERENCES

(1) Jin, R. *Nanoscale* **2010**, *2*, 343.
(2) Lu, Y.; Chen, W. *Chem. Soc. Rev.* **2012**, *41*, 3594.
(3) Yu, Y.; Yao, Q.; Luo, Z.; Yuan, X.; Lee, J. Y.; Xie, J. *Nanoscale* **2013**, *5*, 4606.
(4) Luo, Z.; Nachammai, V.; Zhang, B.; Yan, N.; Leong, D. T.; Jiang, D.-e.; Xie, J. *J. Am. Chem. Soc.* **2014**, *136*, 10577.
(5) Yamazoe, S.; Koyasu, K.; Tsukuda, T. *Acc. Chem. Res.* **2013**, *47*, 816.
(6) Li, G.; Jin, R. *Acc. Chem. Res.* **2013**, *46*, 1749.
(7) Choi, S.; Dickson, R. M.; Yu, J. *Chem. Soc. Rev.* **2012**, *41*, 1867.
(8) Zhu, M.; Aikens, C. M.; Hollander, F. J.; Schatz, G. C.; Jin, R. *J. Am. Chem. Soc.* **2008**, *130*, 5883.
(9) Negishi, Y.; Nobusada, K.; Tsukuda, T. *J. Am. Chem. Soc.* **2005**, *127*, 5261.
(10) Kim, B. H.; Hackett, M. J.; Park, J.; Hyeon, T. *Chem. Mater.* **2014**, *26*, 59.
(11) Luo, Z.; Yuan, X.; Yu, Y.; Zhang, Q.; Leong, D. T.; Lee, J. Y.; Xie, J. *J. Am. Chem. Soc.* **2012**, *134*, 16662.
(12) Yu, Y.; Luo, Z.; Chevrier, D. M.; Leong, D. T.; Zhang, P.; Jiang, D.-e.; Xie, J. *J. Am. Chem. Soc.* **2014**, *136*, 1246.
(13) Knoppe, S.; Bürgi, T. *Acc. Chem. Res.* **2014**, *47*, 1318.
(14) Wang, S.; Meng, X.; Das, A.; Li, T.; Song, Y.; Cao, T.; Zhu, X.; Zhu, M.; Jin, R. *Angew. Chem., Int. Ed.* **2014**, *53*, 2376.
(15) Chong, H.; Li, P.; Wang, S.; Fu, F.; Xiang, J.; Zhu, M.; Li, Y. *Sci. Rep.* **2013**, *3*, 3214.
(16) Chen, Y.-S.; Kamat, P. V. *J. Am. Chem. Soc.* **2014**, *136*, 6075.
(17) Yuan, X.; Zhang, B.; Luo, Z.; Yao, Q.; Leong, D. T.; Yan, N.; Xie, J. *Angew. Chem., Int. Ed.* **2014**, *53*, 4623.
(18) Wu, Z.; Jin, R. *Nano Lett.* **2010**, *10*, 2568.
(19) Mathew, A.; Natarajan, G.; Lehtovaara, L.; Häkkinen, H.; Kumar, R. M.; Subramanian, V.; Jaleel, A.; Pradeep, T. *ACS Nano* **2013**, *8*, 139.
(20) Niihori, Y.; Matsuzaki, M.; Pradeep, T.; Negishi, Y. *J. Am. Chem. Soc.* **2013**, *135*, 4946.
(21) Tracy, J. B.; Crowe, M. C.; Parker, J. F.; Hampe, O.; Fields-Zinna, C. A.; Dass, A.; Murray, R. W. *J. Am. Chem. Soc.* **2007**, *129*, 16209.
(22) Tracy, J. B.; Kalyuzhny, G.; Crowe, M. C.; Balasubramanian, R.; Choi, J.-P.; Murray, R. W. *J. Am. Chem. Soc.* **2007**, *129*, 6706.
(23) Dolamic, I.; Knoppe, S.; Dass, A.; Bürgi, T. *Nat. Commun.* **2012**, *3*, 798.
(24) Kwak, K.; Kumar, S. S.; Pyo, K.; Lee, D. *ACS Nano* **2013**, *8*, 671.
(25) Kwak, K.; Lee, D. *J. Phys. Chem. Lett.* **2012**, *3*, 2476.
(26) Kim, H.; Carney, R. P.; Reguera, J.; Ong, Q. K.; Liu, X.; Stellacci, F. *Adv. Mater.* **2012**, *24*, 3857.
(27) Nikolic, M. S.; Olsson, C.; Salcher, A.; Kornowski, A.; Rank, A.; Schubert, R.; Frömsdorf, A.; Weller, H.; Förster, S. *Angew. Chem., Int. Ed.* **2009**, *48*, 2752.
(28) Edmonds, W. F.; Li, Z.; Hillmyer, M. A.; Lodge, T. P. *Macromolecules* **2006**, *39*, 4526.
(29) Jakobs, R. T. M.; van Herrikhuyzen, J.; Gielen, J. C.; Christianen, P. C. M.; Meskers, S. C. J.; Schenning, A. P. H. J. *J. Mater. Chem.* **2008**, *18*, 3438.
(30) Zubarev, E. R.; Xu, J.; Sayyad, A.; Gibson, J. D. *J. Am. Chem. Soc.* **2006**, *128*, 15098.
(31) Song, Y.; Chen, S. *Langmuir* **2014**, *30*, 6389.
(32) Song, J.; Cheng, L.; Liu, A.; Yin, J.; Kuang, M.; Duan, H. *J. Am. Chem. Soc.* **2011**, *133*, 10760.
(33) van Herrikhuyzen, J.; Portale, G.; Gielen, J. C.; Christianen, P. C. M.; Sommerdijk, N. A. J. M.; Meskers, S. C. J.; Schenning, A. P. H. J. *Chem. Commun.* **2008**, 697.
(34) Jadzinsky, P. D.; Calero, G.; Ackerson, C. J.; Bushnell, D. A.; Kornberg, R. D. *Science* **2007**, *318*, 430.
(35) Heaven, M. W.; Dass, A.; White, P. S.; Holt, K. M.; Murray, R. W. *J. Am. Chem. Soc.* **2008**, *130*, 3754.
(36) Desireddy, A.; Conn, B. E.; Guo, J.; Yoon, B.; Barnett, R. N.; Monahan, B. M.; Kirschbaum, K.; Griffith, W. P.; Whetten, R. L.; Landman, U.; Bigioni, T. P. *Nature* **2013**, *501*, 399.
(37) Yang, H.; Wang, Y.; Huang, H.; Gell, L.; Lehtovaara, L.; Malola, S.; Häkkinen, H.; Zheng, N. *Nat. Commun.* **2013**, *4*, 2422.
(38) Yang, H.; Wang, Y.; Yan, J.; Chen, X.; Zhang, X.; Häkkinen, H.; Zheng, N. *J. Am. Chem. Soc.* **2014**, *136*, 7197.
(39) Yao, Q.; Luo, Z.; Yuan, X.; Yu, Y.; Zhang, C.; Xie, J.; Lee, J. Y. *Sci. Rep.* **2014**, *4*, 3848.
(40) Crasto, D.; Malola, S.; Brosofsky, G.; Dass, A.; Häkkinen, H. *J. Am. Chem. Soc.* **2014**, *136*, 5000.
(41) Pradhan, S.; Xu, L.; Chen, S. *Adv. Funct. Mater.* **2007**, *17*, 2385.
(42) Zubarev, E. R.; Xu, J.; Sayyad, A.; Gibson, J. D. *J. Am. Chem. Soc.* **2006**, *128*, 4958.
(43) Woehrle, G. H.; Warner, M. G.; Hutchison, J. E. *J. Phys. Chem. B* **2002**, *106*, 9979.
(44) Shichibu, Y.; Negishi, Y.; Tsukuda, T.; Teranishi, T. *J. Am. Chem. Soc.* **2005**, *127*, 13464.
(45) Dass, A.; Stevenson, A.; Dubay, G. R.; Tracy, J. B.; Murray, R. W. *J. Am. Chem. Soc.* **2008**, *130*, 5940.
(46) Qian, H.; Zhu, Y.; Jin, R. *ACS Nano* **2009**, *3*, 3795.
(47) Yuan, X.; Luo, Z.; Yu, Y.; Yao, Q.; Xie, J. *Chem.—Asian J.* **2013**, *8*, 858.
(48) Dou, X.; Yuan, X.; Yu, Y.; Luo, Z.; Yao, Q.; Leong, D. T.; Xie, J. *Nanoscale* **2013**, *6*, 157.
(49) Yao, Q.; Yu, Y.; Yuan, X.; Yu, Y.; Xie, J.; Lee, J. Y. *Small* **2013**, *9*, 2696.
(50) Yuan, X.; Luo, Z.; Zhang, Q.; Zhang, X.; Zheng, Y.; Lee, J. Y.; Xie, J. *ACS Nano* **2011**, *5*, 8800.
(51) Yuan, X.; Yu, Y.; Yao, Q.; Zhang, Q.; Xie, J. *J. Phys. Chem. Lett.* **2012**, *3*, 2310.
(52) Tiddy, G. J. T. *Phys. Rep.* **1980**, *57*, 1.
(53) Svenson, S. *Curr. Opin. Colloid Interface Sci.* **2004**, *9*, 201.
(54) Yang, J.; Lee, J. Y.; Ying, J. Y. *Chem. Soc. Rev.* **2011**, *40*, 1672.
(55) Yang, J.; Sargent, E.; Kelley, S.; Ying, J. Y. *Nat. Mater.* **2009**, *8*, 683.
(56) Zhu, Y.; Qian, H.; Drake, B. A.; Jin, R. *Angew. Chem., Int. Ed.* **2010**, *49*, 1295.
(57) Szoka, F.; Papahadjopoulos, D. *Annu. Rev. Biophys. Bioeng.* **1980**, *9*, 467.
(58) Chen, F.; Xu, G.-Q.; Hor, T. S. A. *Mater. Lett.* **2003**, *57*, 3282.
(59) Cheng, W.; Dong, S.; Wang, E. *Langmuir* **2003**, *19*, 9434.
(60) Li, Z.; Zhang, J.; Du, J.; Han, B.; Mu, T.; Gao, Y.; Liu, Z. *Mater. Chem. Phys.* **2005**, *91*, 40.
(61) Pashley, R. M.; McGuiggan, P. M.; Horn, R. G.; Ninham, B. W. *J. Colloid Interface Sci.* **1988**, *126*, 569.
(62) Zhu, M.; Chan, G.; Qian, H.; Jin, R. *Nanoscale* **2011**, *3*, 1703.
(63) Kauffman, D. R.; Alfonso, D.; Matranga, C.; Li, G.; Jin, R. *J. Phys. Chem. Lett.* **2012**, *4*, 195.

DOI: 10.1021/jacs.5b00090
J. Am. Chem. Soc. 2015, 137, 2128−2136